frontiers in Earth Science

ORIGINAL RESEARCH
published: 03 March 2022
doi: 10.3389/feart.2022.860952

Geological Characteristics and Controlling Factors of Enrichment of Deep Shale Gas in the East Weiyuan–North Rongchang Area, Sichuan Basin, China

Yijia Wu[1,2], Hongming Tang[1]*, Jing Li[2], Zhi Gao[2], Bei Yang[2], Cheng Yang[2] and Tian Tang[2]*

[1]School of Geoscience and Technology, Southwest Petroleum University, Chengdu, China, [2]Institute of Geological Exploration and Development of CNPC Chuanqing Drilling Engineering, Chengdu, China

OPEN ACCESS

Edited by:
Shuai Yin,
Xi'an Shiyou University, China

Reviewed by:
Yue Qingyou,
Liaoning Shihua University, China
Yang Wang,
China University of Petroleum, Beijing, China

***Correspondence:**
Yijia Wu
wuyj_dyy@cnpc.com.com
Hongming Tang
swpithm@vip.163.com

Specialty section:
This article was submitted to Economic Geology, a section of the journal Frontiers in Earth Science

Received: *24 January 2022*
Accepted: *15 February 2022*
Published: *03 March 2022*

Citation:
Wu Y, Tang H, Li J, Gao Z, Yang B, Yang C and Tang T (2022) Geological Characteristics and Controlling Factors of Enrichment of Deep Shale Gas in the East Weiyuan–North Rongchang Area, Sichuan Basin, China. Front. Earth Sci. 10:860952. doi: 10.3389/feart.2022.860952

The southern Sichuan Basin is the core area of China's efficient development of deep shale gas (burial depth greater than 3,500 m). Reservoir geological characteristics determine whether shale gas can be preserved, enriched, and produced. Taking the Long 1_1 submember of the Wufeng Formation of the Upper Ordovician and the Longmaxi Formation of the Lower Silurian in the East Weiyuan–North Rongchang area as an example, we used the core, logging, production test, and other data, combining X-ray diffraction analysis, LECO Total Organic Carbon (TOC)-S analysis, optical microscopy, and argon ion polishing field-emission scanning electron microscopy, to study the shale mineral composition, geochemistry, reservoir space, pore structure characteristics, and reservoir physical properties. The following results were obtained: 1) The brittle mineral content, organic matter maturity, and TOC content are high, gradually increase from top to bottom, and reach their maxima at small layer 1 of Long 1_1. 2) Organic pores, inorganic pores, and fractures are important reservoir spaces, among which organic pores and fractures are important seepage channels for shale gas. 3) The shale pore structure revealed by electron microscopy shows that the pore structure in target layers can be divided into four types: unimodal type (mainly organic pores), bimodal type (both organic and inorganic pores), monoclinic type I (mainly organic pores), and monoclinic type II (mainly inorganic pores). The pore morphology is complex, and circular and oval shapes predominate. 4) Sedimentary facies are the main factor controlling the enrichment of shale gas, and the development of fractures is the key to obtaining high yields of shale gas. 5) The class I favorable target area is mainly distributed in wells W206, W206H1, R234H, and R233H and areas to its south, and some areas in the east of the study area.

Keywords: deep shale gas, geological characteristics, reservoir characteristics, Enrichment and high yield, controlling factors, pore structure, East-Weiyuan-north Rongchang area

INTRODUCTION

The marine shale gas resources in China are abundant. Reservoir geological characteristics have always been a hot topic in shale gas exploration and development in China and abroad since they play an important role in controlling the enrichment and production of shale gas (Fan et al., 2018; Li et al., 2019; Fan et al., 2020a; Fan et al., 2020b; He et al., 2021a). The favorable areas for marine shale gas are mainly located in Sichuan Basin, China. The main strata are the Wufeng Formation of the Upper Ordovician–Longmaxi Formation of the Lower Silurian, the main burial depth being 3,500–4,500 m. Shale gas areas have been found successively, such as Luzhou, Changning, Weiyuan, Fuling, and Dingshan, and breakthroughs in exploration and development have been made. The proven geological reserves in China are approximately $2.0 \times 1012\ m^3$. Their output is approximately $154 \times 108\ m^3$, making China the second-largest shale gas producer in the world (Nie and Jin, 2016; Nie et al., 2018; Zhang F. et al., 2020; He et al., 2021b).

The shale gas exploration technology for burial depths less than 3,500 m is well developed, forming a comprehensive geological evaluation technology of shale reservoirs that effectively guides the large-scale industrial development of medium–shallow shale gas. With the deepening of shale gas exploration and development, deep shale with burial depth greater than 3,500 m is widely distributed, with extensive resources (for example, the amount of deep shale gas in southern Sichuan is as high as $8 \times 1012\ m^3$) (Liu Y. J. et al., 2021; Li W. G. et al., 2021; Liu Y. Y. et al., 2021; Ma et al., 2021). Therefore, the development of geological theories related to the enrichment and production of deep shale gas has strategic significance for ensuring national energy security. Compared with shallow shale gas fields, there are obvious differences in geological engineering conditions of deep shale gas fields in China. For example, deep shale gas fields are mostly located in complex structural areas, with complex fold and fault relations, large *in situ* stress and stress differences, and high temperatures and pressures, so the main technologies suitable for shallow shale gas exploration and development are no longer adequate (Zhao et al., 2020; Zhang BL. et al., 2020, Zhang DD. et al., 2020; Xu F. S. et al., 2021; Xi et al., 2021a, Xi et al., 2021b). Previous studies have made great progress in understanding the geological characteristics of shale reservoirs; defined the geochemical characteristics, mineralogical characteristics, and reservoir space characteristics of the reservoirs; found that the sedimentary environment, organic matter (OM), clay minerals, brittle minerals, and fractures are the main controlling factors of shale reservoir yields; and formed a comprehensive research system for shale reservoirs (Chen et al., 2016; Li et al., 2019c; Chen S. L. et al., 2020; Li et al., 2020; Liu et al., 2020; Chen et al., 2021a; Chen et al., 2021b; Liu J. et al., 2021; Sun, 2021). However, these research results and conclusions apply mainly to shallow shale gas with a burial depth of less than 3,500 m. Due to the influence of sedimentation, diagenesis, and tectonism, deep shale gas reservoirs have higher contents of brittle minerals, more developed natural fractures, and more complex pore evolution, resulting in different shale geological characteristics and controlling factors for shale gas enrichment and yield (Yin et al., 2019; Chen F. et al., 2020; Chai et al., 2020; Xu and Gao, 2020; Yin and Wu, 2020; Zhou et al., 2020; Song et al., 2021; Tabatabaei 2021). Therefore, clarifying the geological characteristics of deep shale is needed to explore and extract deep shale gas.

The burial depth of the main shale in the East Weiyuan–North Rongchang area is 3,800–4,300 m, so the shale reservoir characteristics and the state of the shale gas and its preservation conditions are significantly different from those of medium–shallow shale gas. It is a typical area to analyze the geological characteristics and controlling factors of deep shale gas (Xiong et al., 2021; Zhao et al., 2021; Zhou et al., 2021). Therefore, we used the data from logging, core, seismic, and experimental tests to comprehensively analyze the rock and mineral characteristics, reservoir space characteristics, organic geochemical characteristics, and physical properties of high-quality deep shale reservoirs in the East Weiyuan–North Rongchang to clarify the main controlling factors of deep shale gas enrichment and high yield. We then calculated the optimal target areas, thus providing guidance for exploring and developing regional deep shale gas in this study area and similar areas.

GEOLOGICAL SETTING

The East Weiyuan–North Rongchang block is located in the Central South of Sichuan Basin. The East Weiyuan block is located in the middle-slope gentle belt of the Central Sichuan Paleo-uplift and the low-fold belt of the Southwest Sichuan Paleo-uplift. North Rongchang block is located in the middle-slope gentle belt of Central Sichuan Paleo-uplift and the low steep bend belt of the Central Sichuan Paleo-depression. The structure of the study area is relatively simple. The Northern and Western areas consist of gentle, low-amplitude, monoclinic, or nasal protrusion-like structures, with undeveloped faults, and only some small-scale faults are developed. The Zhongaoxi buried structure is in the middle, the Luoguanshan structure is in the south, and the Xishan structure is connected in the east, showing the structural characteristics of a wide syncline and a narrow anticline. Faults are developed and mostly distributed in the NE–SW direction (**Figure 1**) (Wu et al., 2021; Zhao et al., 2021). The Late Ordovician–Early Silurian is the turning period of sedimentary-tectonic evolution of the Yangtze Block. Dominated by rising sea level, the East Weiyuan–North Rongchang area forms a detention basin, which inundates the carbonate platform and provides conditions for the deposition of black shale of the Ordovician Wufeng Formation and the Longmaxi Formation at the bottom of the Lower Silurian. Overall, the Wufeng Formation–Longmaxi Formation is mainly continental shelf facies in the study area. The shelf environment consists of an inner shelf close to the shore and far away. The upper limit is near the normal wave level, and the lower water depth limit is generally approximately 200 m (Liu S. G. et al., 2021; Liu Q. Y. et al., 2021). The Wufeng Formation–Longmaxi Formation is close to the shore facies in the landward direction on the plane, and the sediments are mainly dark mud debris.

The oldest stratum exposed on the surface of the study area is the 1 Triassic Xujiahe formation, and the top is the Shaximiao Formation. The drilling data show that the stratigraphic sequence

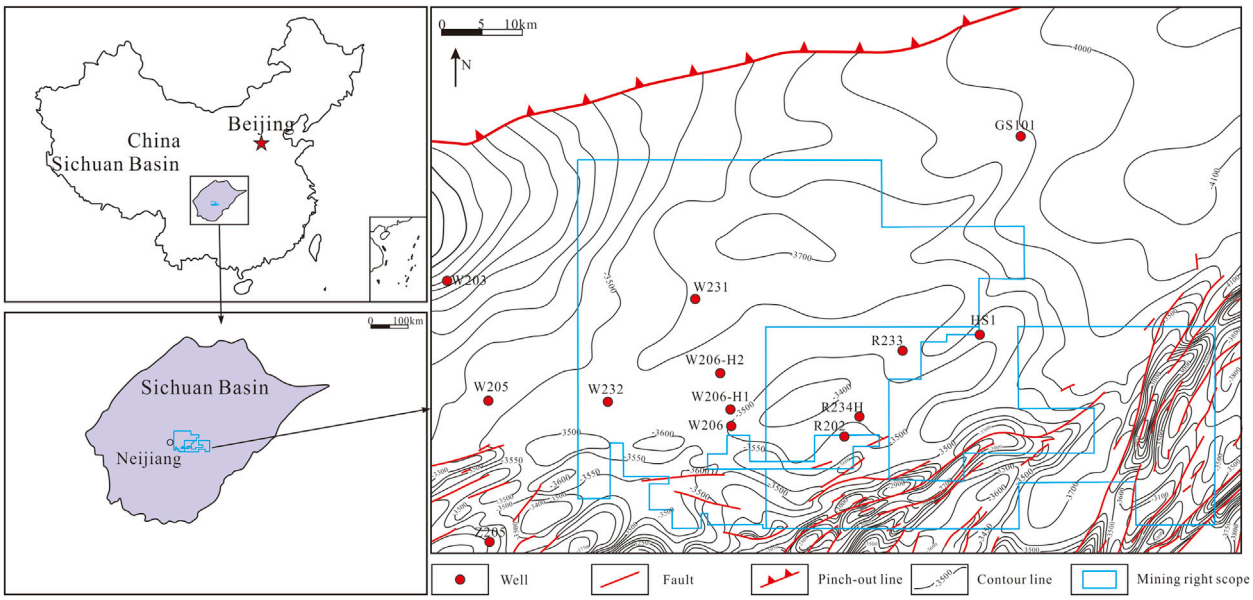

FIGURE 1 | Seismic reflection structure of the Upper Ordovician top boundary in the study area.

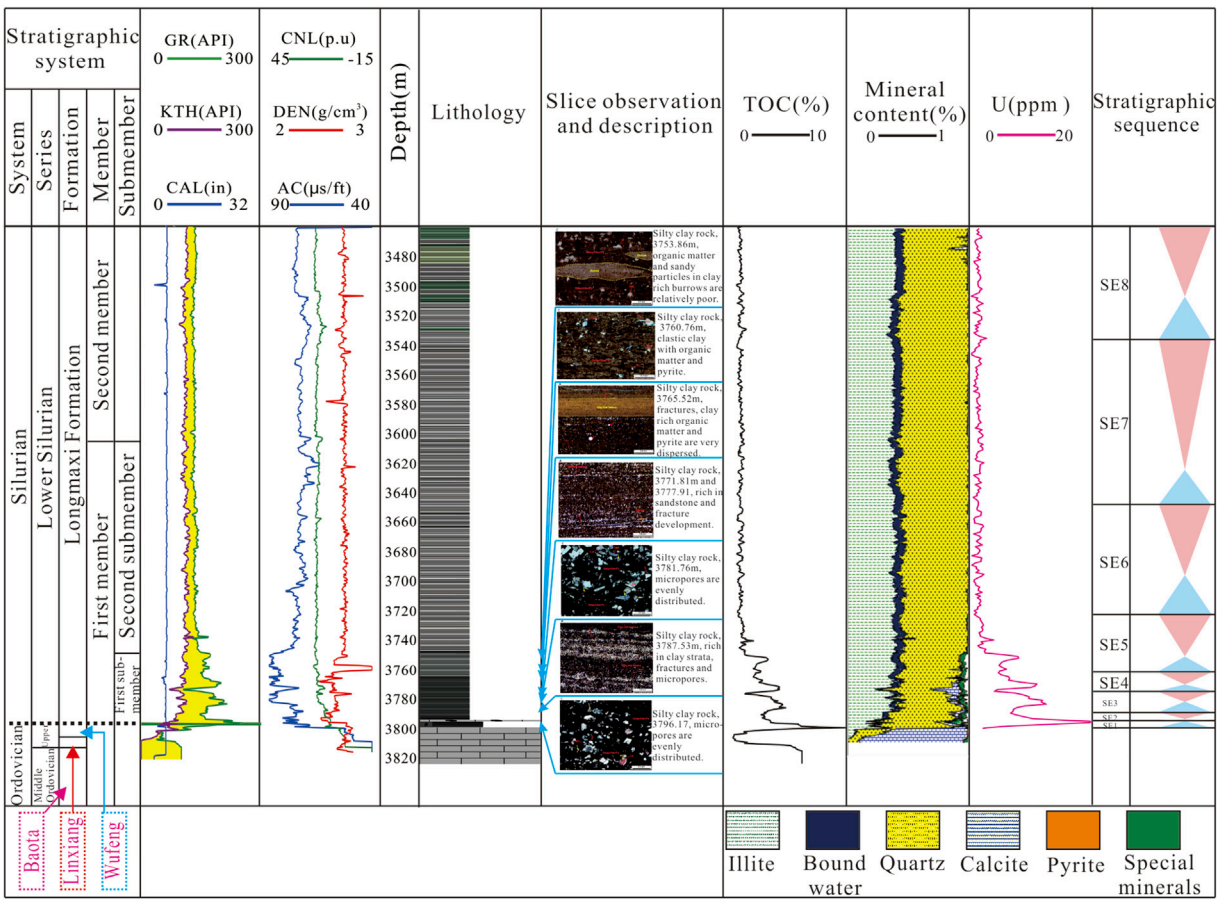

FIGURE 2 | Comprehensive histogram of the Longmaxi Formation of well W206.

from top to bottom is normal. The stratigraphic thickness of the Lower Silurian Longmaxi Formation is 283–515 m, which is in conformable contact with the overlying Shiniulan Formation. At the bottom, there is a clear boundary between the black carbonaceous shale containing carbonate rock and the grayish-brown biological limestone of the Guanyinqiao Section of the Wufeng Formation of the Lower Ordovician, forming a pseudo-conformable contact. The rock color gradually deepens from top to bottom. The upper part is grayish-green and greenish-gray shale. The middle and lower parts are grayish-black to black calcareous and carbonaceous shale, which generally is calcareous, silty, dense, and brittle, and the foliation is relatively developed (leaf bedding). The natural gamma ray is serrated, mostly with high values. The bottom is obviously uplifted compared with the upper part, with a value of 140–500 API. The Longmaxi Formation can be divided into upper and lower segments, namely, the Long 1 member and the Long 2 member. The Long 1 member can be divided into upper and lower subsegments, namely, Long 1_2 and long 1_1. Long 1_1 can be divided into four small layers, the main shale gas-producing layers (**Figure 2**).

SAMPLES AND EXPERIMENTS

Experimental Samples

The shale of the Wufeng Formation–Longmaxi Formation in the East Weiyuan–North Rongchang block was deposited in an organic-rich shelf environment (Wu et al., 2021; Zhao et al., 2021). In this study, conventional logging and imaging logging data of eight wells, including R202, R233H, W231, W232, and W206, were collected to analyze the characteristics of the reservoir lithology, reservoir space, brittle minerals, and gas-bearing. At the same time, 52 samples of five wells of Long 1_1 sub-member were collected, including 10 shales in small layer 1, 15 shales in small layer 2, eight shale in small layer 3, and 19 shales in small layer 4.

X-Ray Diffraction Analysis

The 52 samples were crushed and passed through a 200-mesh sieve. After drying, a certain number of samples were taken and analyzed by a Bruker D8 X-ray diffractometer. The working voltage was 40 kV, the current was 30 mA, and the scanning was conducted at 4°/min. Determinations were made according to the *Inorganic chemicals for industrial use-Crystal form analysis-X-ray diffraction method* (GB/T 30904-2014). The main peak area of each mineral was used to calculate the relative content (Cai et al., 2020).

Geochemical Characteristic Analysis

The OM maturity and abundance are key geochemical characteristics of shale. Since there is no vitrinite in the highly mature source rocks of the Lower Paleozoic, the maturity of the Lower Paleozoic source rocks cannot be evaluated by vitrinite reflectance (Shi et al., 2016; Yu H. et al., 2017; Rui et al., 2019; Wang et al., 2019). In this study, the maturity of the Lower Paleozoic source rocks was evaluated by studying the correlation between solid asphalt and vitrinite reflectance, fitting the conversion formula between asphalt reflectance and vitrinite reflectance, and converting the asphalt reflectance into vitrinite reflectance.

Total organic carbon (TOC) content can better characterize the OM abundance. In this study, 52 samples were crushed and passed through a 200-mesh sieve. After drying at low temperature, the carbonate minerals were removed with dilute hydrochloric acid. According to the Determination of total organic carbon in sedimentary rock (GB/T 19145-2003), the TOC content was determined with a LECO CS230 carbon/sulfur determinator (Wang et al., 2016; Zhao et al., 2017; Cai et al., 2020).

Observation by Argon Ion Polishing Field-Emission Scanning Electron Microscopy

Representative core samples from five wells were selected for SEM observation according to our core observation. First, the experimental samples were polished by argon-ion, and then small shale samples were cut into regular cuboids and put into the injection chamber of the polisher. They were bombarded with argon ions in a vacuum for 2 h, and then the SU8010 FESEM has used under the secondary electron (SE)/backscattered electron (BSE) mode. The observation was carried out to obtain images of complete shales.

RESULTS

Mineral Composition Characteristics

The XRD analysis of the first segment of the Wufeng Formation–Longmaxi Formation in the study area shows that minerals are mainly quartz, feldspar, calcite, dolomite, and clay minerals, and pyrite and marcasite contents are scarce. The brittle minerals are primarily quartz, feldspar, carbonate minerals, pyrite, and hematite, showing a gradually increasing trend from top to bottom in the vertical direction, and the content of brittle minerals peaks at small layer 1 (**Figures 3A,B**). Specifically, the content of brittle minerals in the Wufeng Formation is 62.6–89.9%, with an average of 74.9%; in small layer 1, 55.3–76.4% with an average of 64.4%; in small layer 2, 60.3–79% with an average of 67.5%; in small layer 3, 49.9–74.5% with an average of 60.2%; and in small layer 4, 45.2–72% with an average of 58.3% (**Figure 3C**). In terms of plane distribution, each well's measured brittle mineral content is generally stable, with an average greater than 60%. The brittle mineral content of the Wufeng Formation Long 1_1 sub-member reservoir increases in the east and south directions. The high-value area is distributed from well W206-H2 to well R202, the content gradually decreases toward the surrounding well area, Well W231 is a relatively low-value area, and the compressibility of shale reservoir is generally good (Zhou et al., 2016; Zhang et al., 2019; Zhu et al., 2019; Zhang et al., 2021).

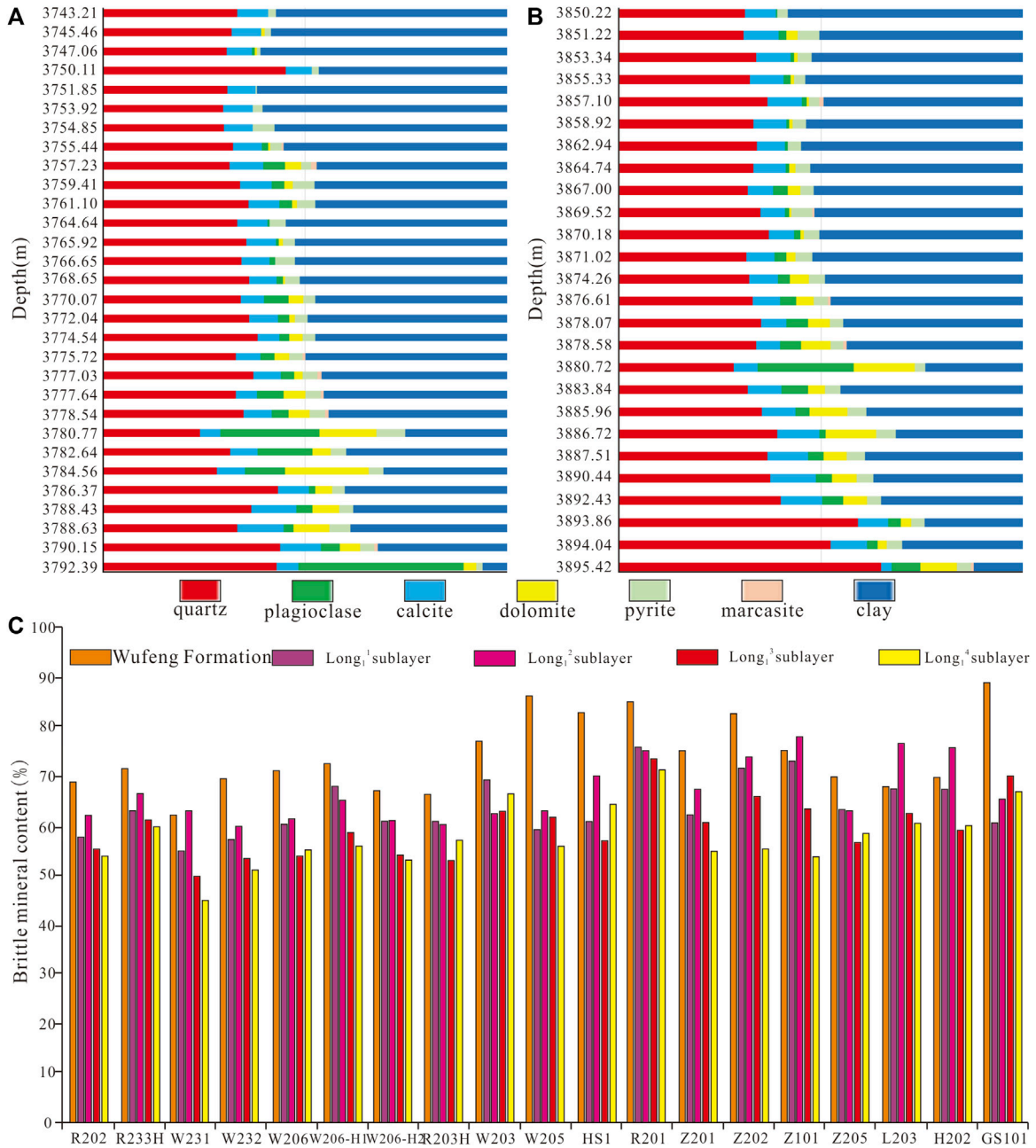

FIGURE 3 | Mineral composition in Wufeng Formation Long 1_1 sub-member in the study area. **(A)**. R233H. **(B)**. Well W206-H2. **(C)**. Brittle mineral content in the study area and adjacent areas.

TABLE 1 | OM maturity in the core analysis of sub-member Long 1_1 in the study area.

Test unit	Test method	Test data points	R_o	W231	W206-H2	R233H	W206
Collett	Conversion of asphalt reflectance	115	R_o Range (%)	2.08–2.38	2.2–2.29	2.1–2.25	-
			R_o Average (%)	2.24	2.24	2.18	-
Core lab	Graptolite reflectance measurement	303	R_o Range (%)	2.1–4	2.2–3.5	2.9–4.9	2.7–3.4
			R_o Average (%)	3	3	3.5	3

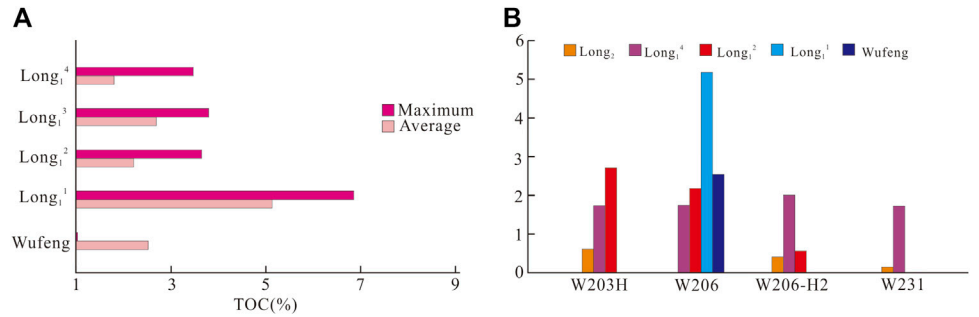

FIGURE 4 | Analysis of TOC content of each small layer by core of the Wufeng Formation Long 1_1 sub-member in the study area.

Geochemical Characteristics

The observation of cores and thin sections shows that there is no vitrinite in the highly mature source rocks of the Lower Paleozoic in the study area, only solid asphalt, which is the residue left after the gas generation of crude oil (He X. et al., 2021; He et al., 2021d; Yuan et al., 2021). Therefore, according to the correlation between solid asphalt and vitrinite reflectance, the maturity of the Lower Paleozoic source rocks can be evaluated after converting asphalt reflectance into vitrinite reflectance. Based on the empirical OM maturity measured by two core analysis methods, the average asphalt reflectance converted into R_o in Long 1_1 is 2.2%. The measured average R_o of graptolite reflectance is 3.1%, and both are over mature stages, mainly producing dry gas (**Table 1**).

To characterize shale OM abundance quantitatively, the LECO CS230 carbon/sulfur analyzer was used to determine the TOC content of gas-bearing shale from Wufeng Formation Long 1_1. The empirical analysis shows that the average TOC of each small layer of Long 1_1 and the Wufeng Formation core is 0.5–2.88%, with small layer 1 having the highest 5.18% (**Figure 4**). Consistent with shallow shale gas, small layer 1 has the highest thermal evolution and OM abundance.

Reservoir Space Characteristics

According to the observation of thin cast sections and the AIP-FESEM of typical samples from five coring wells in the study area, the main reservoir space types of the Wufeng Formation Long 1_1 are organic pores, inorganic pores, and fractures. OM forms organic pores in the later thermal evolution process. Inorganic pores can be further divided into six types (Intergranular pore, Micropore in clay minerals, Intragranular dissolved pore, Intracrystalline dissolved pores, Biological pore, OM pore), mainly including intergranular pores, intercrystalline dissolved pores, and intergranular pores. Fractures mainly include structural and nonstructural fractures, whose development degree is related to the thermal evolution degree of OM, shale brittleness, and tectonic stress. The pore types are mainly micro-nano-pores (Jarvie et al., 2007; Curtis et al., 2012; Zhang K. et al., 2020; Rashid et al., 2020; Xiao et al., 2020; Huang et al., 2021).

1) OM pores

OM pores are the main pore type of shale gas reservoirs. OM pores and their specific surface provide an adsorbent for natural gas and a space for the occurrence of free gas, which is very important for the enrichment of shale gas (Sakhaee-Pour and Bryant, 2015; Guo et al., 2018; Han et al., 2019; Ko, et al., 2017). The development of OM pores is affected by the degree of thermal evolution and the microstructure of the OM, resulting in great differences in the distribution patterns of OM pores in a single vertical well. The study area has a high degree of the thermal evolution of OM. OM pores in various forms are widely distributed. Circular and oval shapes predominate inside them, and sponge, though pore and strip shapes are observed. The pores are irregular, uneven distribution, and the pore diameter is mainly less than 50 nm (**Figures 5A–C**). Longitudinally, the TOC of small layer 1 is the highest, mainly as a sapropel formation, and the developmental degree of OM pores is significantly greater than that of other small layers.

2) Intergranular pores

Compared with conventional oil and gas reservoirs, shale reservoirs have a shallow burial depth and relatively low compaction and diagenesis, and they retain more intergranular pores. Irregular dissolved pores, including mold pores, are formed in feldspar, calcite, dolomite, and other particles. During diagenesis, compaction, and cementation, due to incomplete action, intergranular pores can develop around ductile minerals (clay flocs, microcrystalline spherulite minerals, OM, etc.) and brittle minerals (quartz, feldspar, pyrite, etc.). The pore types are linear and triangular, and the pores are generally larger than OM pores (**Figures 5D–F**).

3) Intercrystalline pores/Intercrystalline dissolved pores

Due to the irregularity of the crystals, brittle and compressive particles, such as pyrite, carbonate, and quartz, it easily form intercrystalline pores in the process of crystal packing in the study area. They are mainly includes pores developed between authigenic crystals, and the pores are clean. Most of these pores are isolated and poorly connected, so it is difficult for natural gas in the source area to flow into these pores (Zou et al., 2010; Yu et al., 2016, Yu Y. X. et al., 2017). Pyrite microspheres formed under an anoxic environment are widely distributed in the study area, present as aggregates of pyrite crystals in a

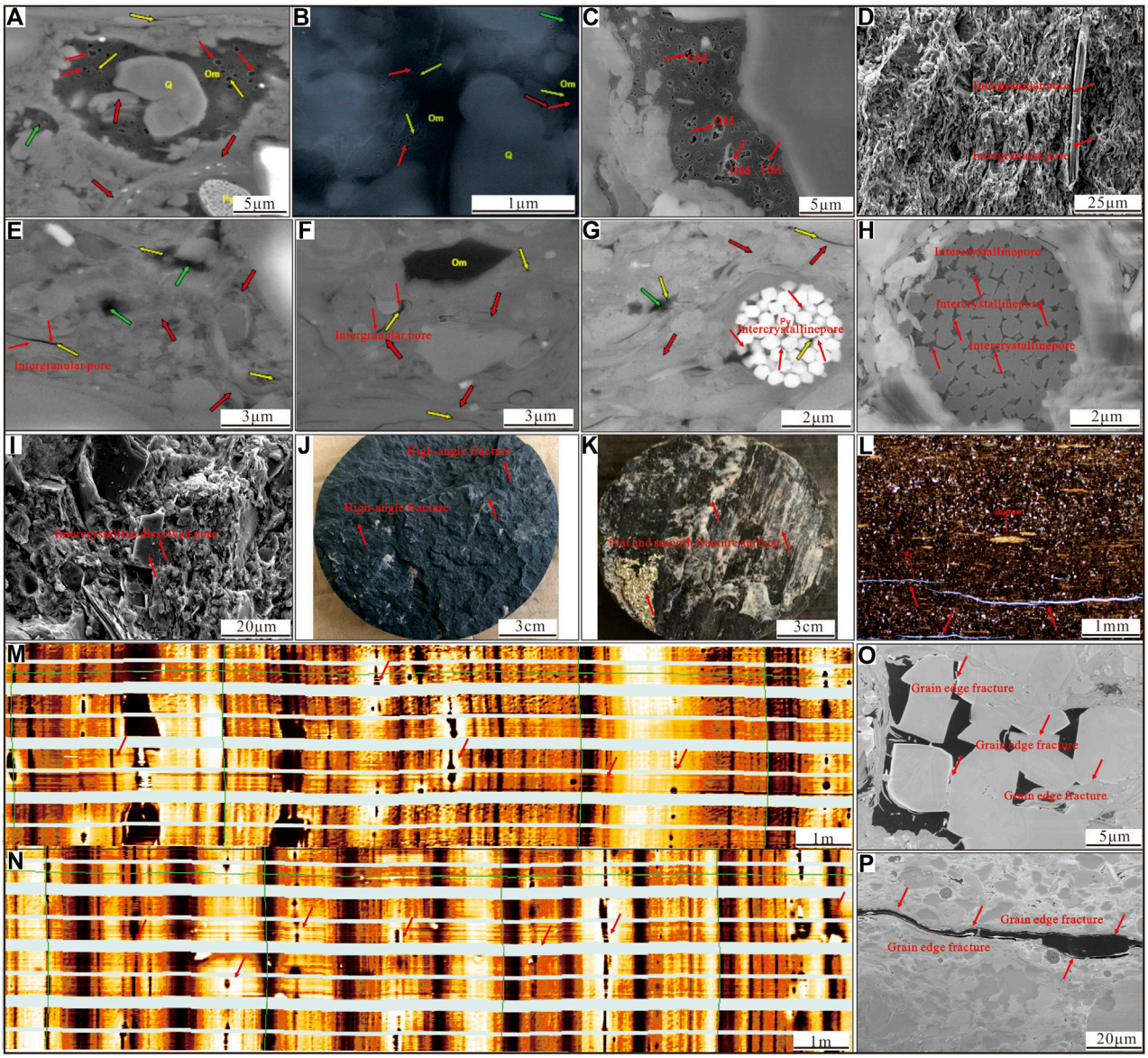

FIGURE 5 | Reservoir space types and characteristics of the Long 1_1 sub-member in the study area. **(A)**. W206, 3,787.53 m, Micropores in organic matter. **(B)**. W206, 3,765.52 m, Micropores in organic matter. **(C)**. R233H, 3,884.35 m, Organic matter pore, The pores are round-oval. **(D)**. W206H2, 3,782.52 m, The intergranular pores are lamellar. **(E)**. W206, 3,771.81 m, Flaky intergranular pores between clay particles. **(F)**. W206, 3,781.76 m, intergranular pores. **(G)**. W206, 3,787.53 m, Intercrystalline pores in pyrite particles. **(H)**. W231, 3,878.92 m, Intercrystalline pores in pyrite particles. **(I)**. R233H, 3,893.50 m, Intercrystalline dissolved pores. **(J)**. W231, 3,878.85 m, Vertical fracture, unfilled. k. R233H, 3,885.27 m, Calcite can be seen on the fracture surface, and there are scratches on the fracture surface. **(L)**. W206, 3,753.86 m, Microcracks parallel to clay bedding. **(M,N)**, characteristics of bedding fractures in the imaging logging. **(O)**. R233H, 3,879.27 m, grain edge fractures. **(P)**. W231, 3,856.62 m, grain edge fractures of organic matter.

raspberry-like shape, and mostly exist individually as regular cube shapes. Due to the non-tight packing during the crystal growth process, the intercrystalline micropores are mostly irregular (**Figures 5G,H**). OM can form many organic acids in hydrocarbon generation, and there are some acidic substances in water formation (Lyu et al., 2021; Wang et al., 2021). These substances migrate under the action of potential energy. They can selectively dissolve feldspar, calcite, and other soluble minerals so that the intercrystalline pores are dissolved in varying degrees, thus forming intercrystalline dissolved pores dominated by ellipses and triangles (**Figure 5I**).

4) Fractures

Shale reservoirs are characterized by ultralow porosity and low permeability. The development of fractures affects the physical

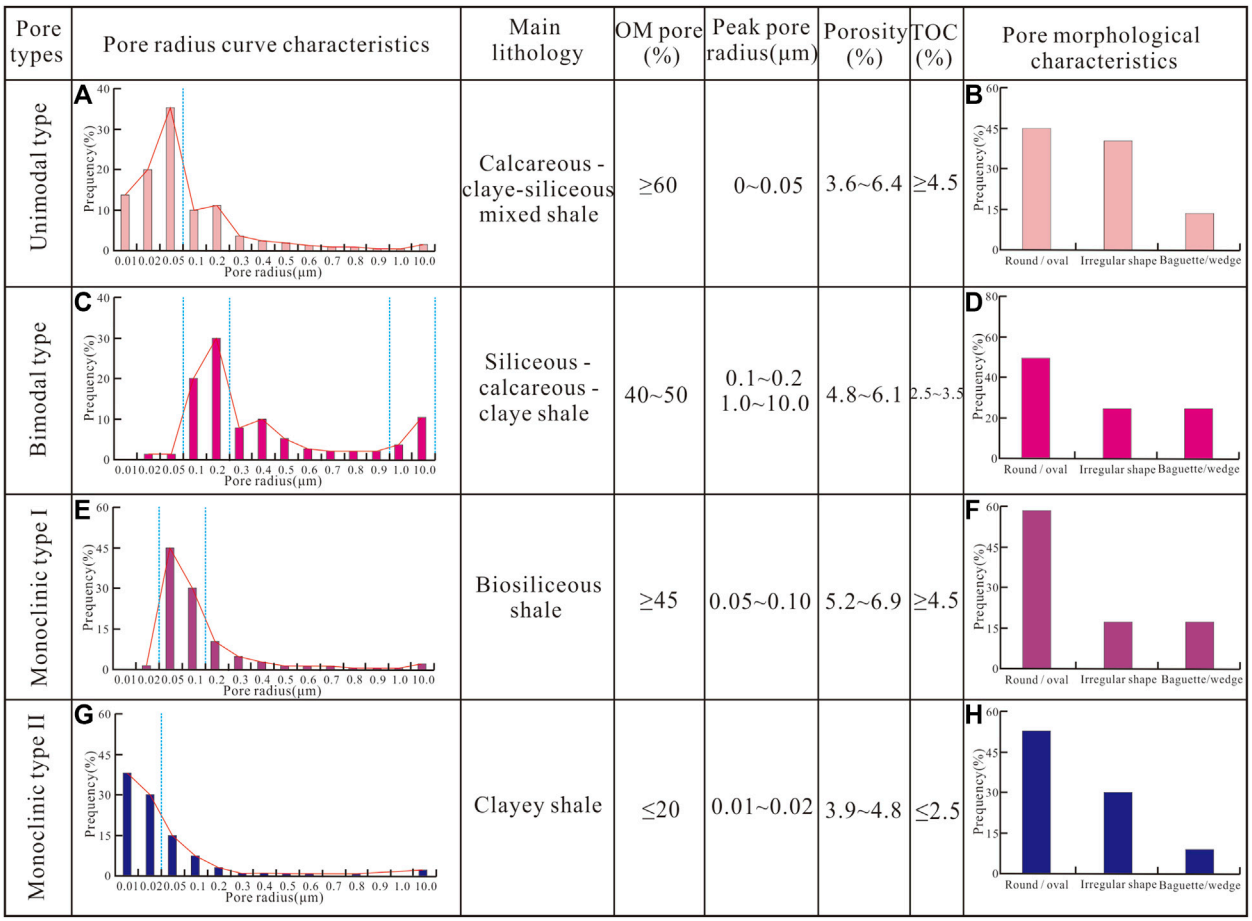

FIGURE 6 | Distribution characteristics of pore structure based on the SEM. **(A)** Pore radius curve characteristics of the unimodal type. **(B)** Pore morphological characteristics of the unimodal type. **(C)** Pore radius curve characteristics of the bimodal type. **(D)** Pore morphological characteristics of the bimodal type. **(E)** Pore radius curve characteristics of the monoclinic type I. **(F)** Pore morphological characteristics of the monoclinic type I. **(G)** Pore radius curve characteristics of the monoclinic type II. **(H)** Pore morphological characteristics of the monoclinic type II.

properties of shale reservoirs and strongly influences the formation and expansion of hydraulic pressure fractures, thus affecting shale productivity. Structural and nonstructural fractures are the main fractures developed in the study area (Zou et al., 2010; Li H. et al., 2021; Li, 2021). Structural fractures are mainly shear fractures formed by structural stress. Our core observation shows that most of them are low-angle and high-angle fractures characterized by flat and smooth fracture surfaces, a regular occurrence, far extension, and more clastic particles (**Figures 5J,K**). Similar characteristics were observed under the electron microscope. Such fractures can better connect poorly interconnected pores, thus greatly improving the seepage capacity of the reservoir (**Figure 5L**). However, if high-angle fractures develop through the layer, this may lead to the loss of shale gas, which is unfavorable to the preservation of shale gas. Foliation bedding fractures are also widely developed in the study area. These fractures show up as dark linear patterns on the map by imaging logging and are mainly the connected organic and inorganic pores in the shale. They can effectively increase the effective porosity of the reservoir, have a great influence on the horizontal seepage capacity of the reservoir (**Figures 5M, N**), and are an important weak surface for the expansion of compression fractures. In addition, microfractures in the study area are extremely well developed, with lengths usually ranging from micrometers to nanometers and widths ranging from hundreds of nanometers to several micrometers. These fractures are of structural origin and nonstructural origin. Fractures with structural origin have characteristics similar to macro-shear fractures (**Figure 5L**), and fractures with nonstructural origin are mainly developed along weak planes dominated by bedding planes and lithologic interfaces, primarily coming in three types: 1) cleavage fractures formed in flake minerals; 2) grain edge fractures formed at the interface between clay minerals and clastic particles (**Figures 5O, P**); and 3) intercrystalline fractures of clay minerals, quartz particles, and pyrite. These microfractures are intertwined into a network, and the joint

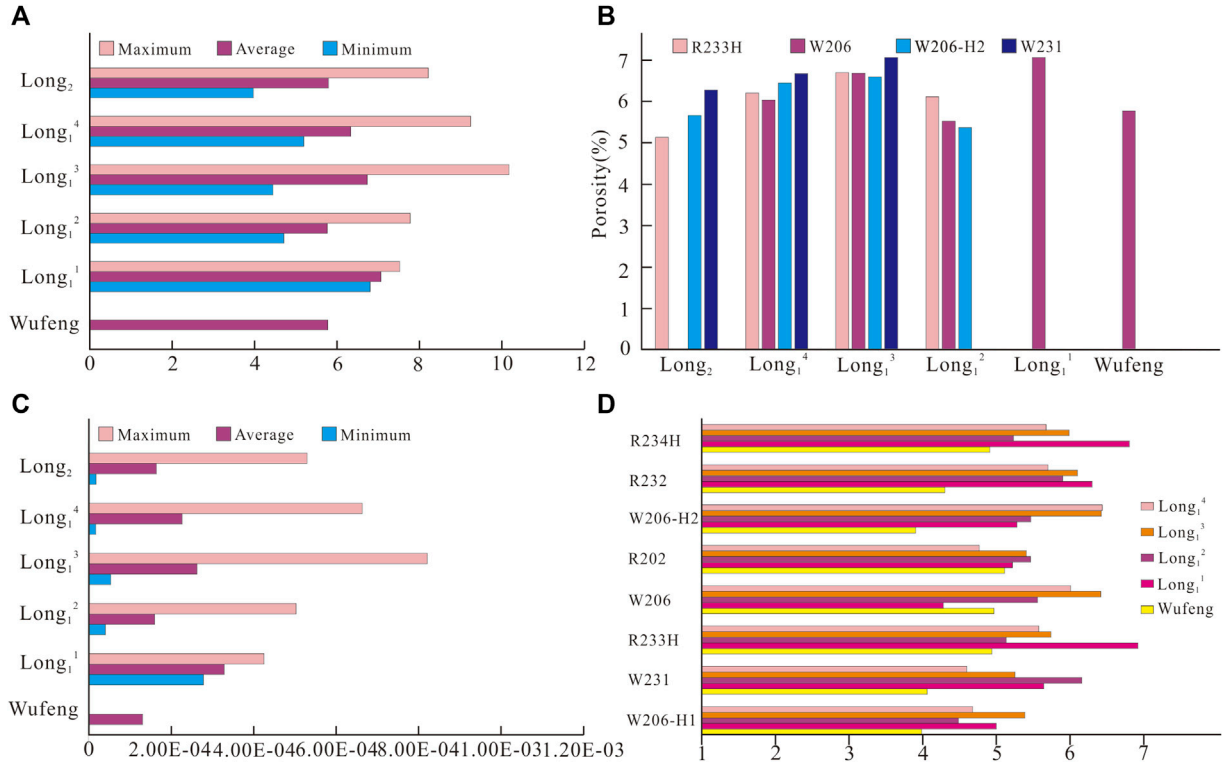

FIGURE 7 | Distribution of porosity and permeability of the Wufeng Formation Long 1_1sub-member in the study area. **(A)** Porosity of each sub-member. **(B)** Porosity of the single well. **(C)** Permeability of each sub-member. **(D)** Permeability of the single well.

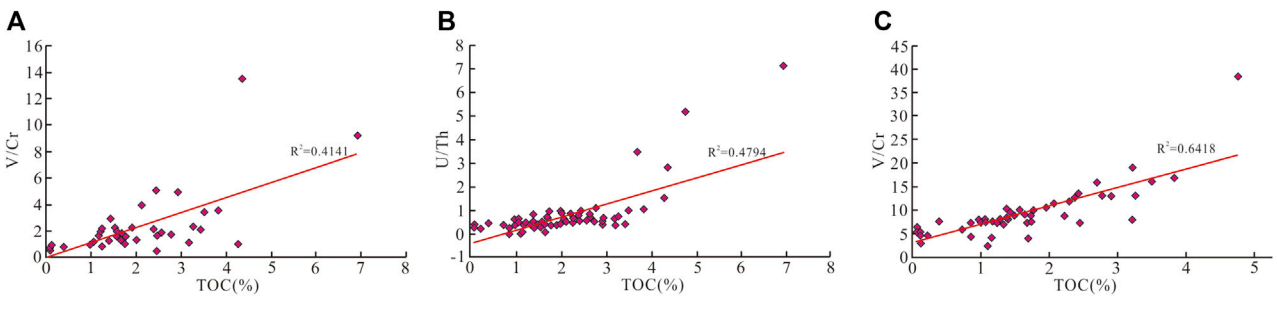

FIGURE 8 | Relationship between TOC content and V/Cr, U/TH, and Ni/CO in the study area.

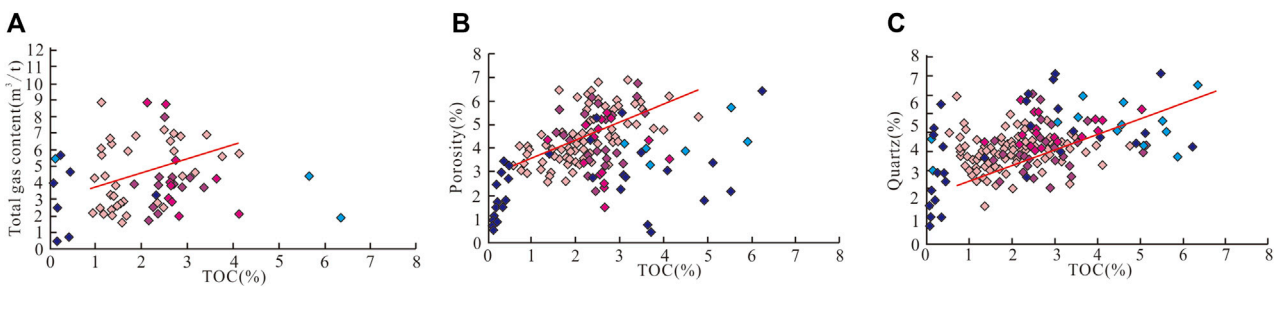

FIGURE 9 | Relationships between TOC content and porosity, gas volume, and quartz in the study area.

TABLE 2 | Sedimentary microfacies of the first member of the wufeng formation–longmaxi formation in the study area.

Subfacies	Microfacies	Horizon	Redox environment	Lithofacies	U/Th	Quartz	Carbonate	Clay	TOC	Porosity	Gas volume	Brittle minerals	Reservoir classification
Outer shelf	Deepwater silty mud shelf	Long 1_1^2, Long 1_1^4	Oxidation, weak local reduction	Ultralow-carbon, low-carbon, and medium-carbon siliceous shale facies; low-carbon and medium-carbon carbonate siliceous shale facies	0.53	41.2	8.91	32.1	2.01	5.57	3.89	56.47	Mainly II, III
	Rich organic silty mud shelf	Long 1_1^3, Wufeng Formation	Oxidation, weak local reduction	Ultralow-carbon, low-carbon, and medium-carbon siliceous shale facies; low-carbon, medium-carbon carbonate siliceous shale facies, low-carbon siliceous carbonate shale facies	0.69	39.57	14.36	27	2.67	5.5	4.33	59.87	Mainly II
	Rich organic mud shelf	Long 1_1^1	Strong reduction	Medium-carbon and high-carbon siliceous shale facies	1.55	48.67	7.69	20.3	4.98	6.27	5.86	62.68	Mainly I
	Rich organic siliceous mud shelf	Long 1_1^1	Strong reduction	High-carbon siliceous shale facies	2.21	45.31	9.86	18.9	5.21	5.68	6.22	59.96	Mainly I

action of micro-and macro fractures has an important impact on the enrichment of shale gas.

Overall, the shale reservoir space of the Longmaxi Formation in the study area is mainly composed of organic pores, inorganic pores, and fractures. Due to the multistage tectonic stress of Indosinian, Yanshan, and Himalayan orogenies, the shale of the Longmaxi Formation has the characteristics of obvious compaction and diagenesis, a high degree of thermal evolution, strong tectonic uplift, and deep burial depth, so OM well-connected pores and fractures are developed in the study area. In contrast, inorganic pores are less developed and poorly connected. Therefore, in the study area, OM pores and fractures are important seepage channels of shale gas.

Pore Structure Characteristics

The SEM analysis of shale pore structure shows that the pore structure of shale reservoirs in the Wufeng Formation Long 1 Member gradually improves from top to bottom. In contrast, the proportion of mesopores (2–50 nm) and large pores (>50 nm) increases, but small pores (<2 nm) and mesopores still predominate, accounting for 42 and 49%, respectively. According to the frequency distribution curve of pore radius, pore structure can be divided into four types (Xiong et al., 2021), i.e., unimodal (mainly organic pores), bimodal (both organic and inorganic pores), monoclinic type I (mainly organic pores), and monoclinic type II (mainly inorganic pores). Their characteristics are as follows.

Unimodal type: There is only one peak frequency of the pore radius. The pore radius has a narrow distribution range, and small pores (micropores) less than 2 nm predominate and are rich in OM (TOC≥4.5%). The lithology is mainly calcareous-clay-siliceous mixed shale. More than 60% of the pores are OM pores. Intergranular pores and intergranular pores are rare, the pores have good sortability and connectivity, and the reservoir has good physical properties (**Figure 6A**). The pore morphology is mainly circular, elliptical, or irregular, together accounting for more than 85%. The pores of other shapes, such as narrow, long, and wedge-shaped, are relatively developed, accounting for approximately 15% (**Figure 6B**).

Bimodal type: There is one peak frequency for the pore radius, the difference between primary and secondary peaks is large, the main peak is approximately 0.1–0.2 μm, and the secondary peak is about 1–10 μm. Pore size varies widely, and mesopores and large pores predominate, with relatively poor sortability and strong heterogeneity. Both organic and inorganic pores are developed, accounting for the same proportion (40–50%), the TOC content is between 2.5 and 3.5%, and the brittle mineral content is high. The organic pore distribution is uneven, the connectivity in general, and the pore structure is slightly worse than that of the unimodal type (**Figure 6C**). The pore morphology is circular and elliptical, accounting for approximately 75%. The proportion of other forms is relatively low, explained by the good compression resistance of rigid particles (**Figure 6D**).

Monoclinic type I: Organic pores predominate, inorganic pores are not developed, and the pore radii are mostly 0.05–0.1 μm. The mesopores predominate, have good sortability, and are rich in OM

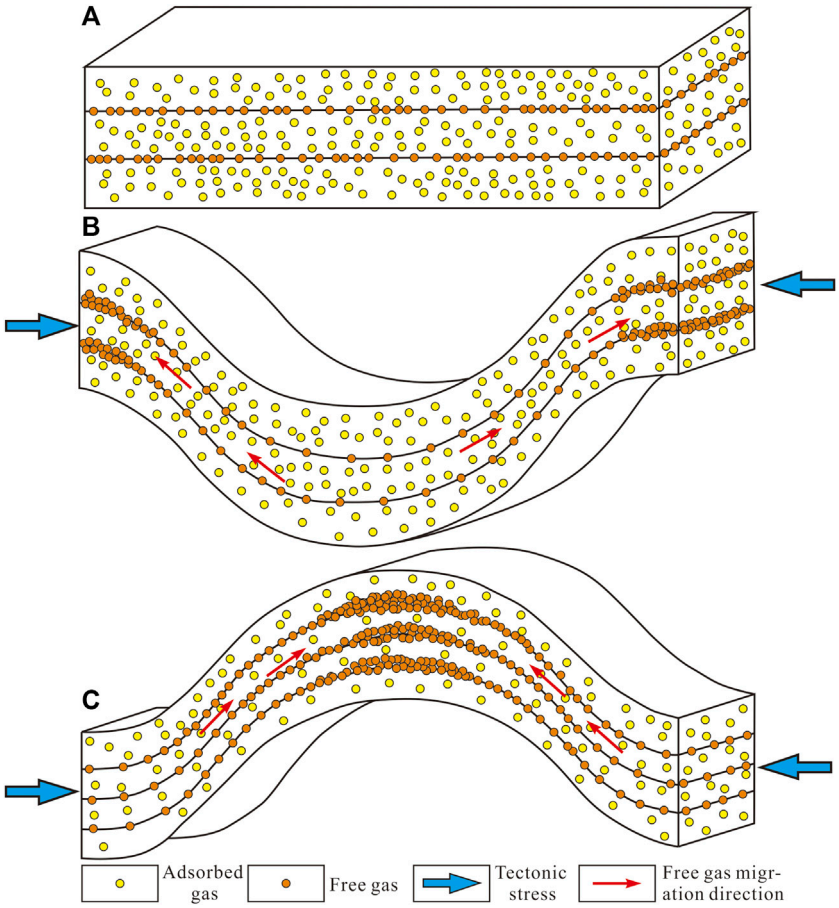

FIGURE 10 | Compound Controlling Mode of Structural Fractures in Shale Gas Reservoirs (Wang et al., 2017; Xu Z. et al., 2021). **(A)**. Model diagram of a shale gas reservoir in North America, with weak structural activity and horizontal fractures. **(B)**. Enrichment model of synclinal gas with no fractures developed at structural highs. **(C)**. Enrichment model of anticlinal gas with no fractures developed at structural highs.

(TOC≥4.5%). The lithology is mainly biological siliceous shale, and pyrite laminae are developed. The pore morphology is mainly circular or oval, accounting for approximately 60%, while irregular, narrow, and wedge-shaped pores account for more than 35%. Siliceous shale has the highest content, the pore radius of organic pores is better than that of unimodal type, and these reservoirs have the best physical properties (**Figures 6E,F**).

Monoclinic Type II: Inorganic pores predominate, organic pores are not developed, and the pore radii are mostly 0.01–0.02 μm. Small pores predominate, with good sortability but poor connectivity and low OM content (TOC<2%). The content of clayey shale is high, pyrite is rare, and round or oval pores account for approximately 55%. They have poor connectivity (**Figures 6G,H**).

Physical Characteristics

Based on the core analysis, vertically, the average core porosity of Long 1_2, each small layer of Long 1_1, and the whole Wufeng Formation is 6.24%, of which small layer 1 has the highest core porosity (7.06%) and Wufeng Formation the lowest (5.77%) (**Figures 7A,B**). Overall, core porosity gradually decreases from bottom to top. The core permeability is 1.33–3.32 × 10^{-4} MD, small layer 1 having the highest and Wufeng Formation the lowest (**Figure 7C**).

The logging results show that the porosity of the Wufeng Formation Long 1_1 sub-member of eight wells in the study area is 4.7–6.0%, with an average of 5.5%. Well W206-H1 had the lowest, Well W206 had the highest, and the distribution is mainly within 5.6–5.8%. Vertically, the porosity trend of each small layer of each well is about the same, of which small layer 3 and small layer 1 have the highest porosity, with an average of 5.84 and 5.68%, respectively, and Wufeng Formation has the lowest, with an average of 4.52% (**Figure 7D**).

The porosity decreases eastward and southward away from the denudation line in the plane distribution. The reservoir area with high porosity is distributed along with the wells W206-H2-R233H-HS1, and well W231 is a relatively low-value area; the reservoir areas with high porosity in small layer 1 are in wells W206, W205 to the northwest, and well WL203 to the south. Overall, the porosity increases with greater formation burial depth and gradually decreases to the south.

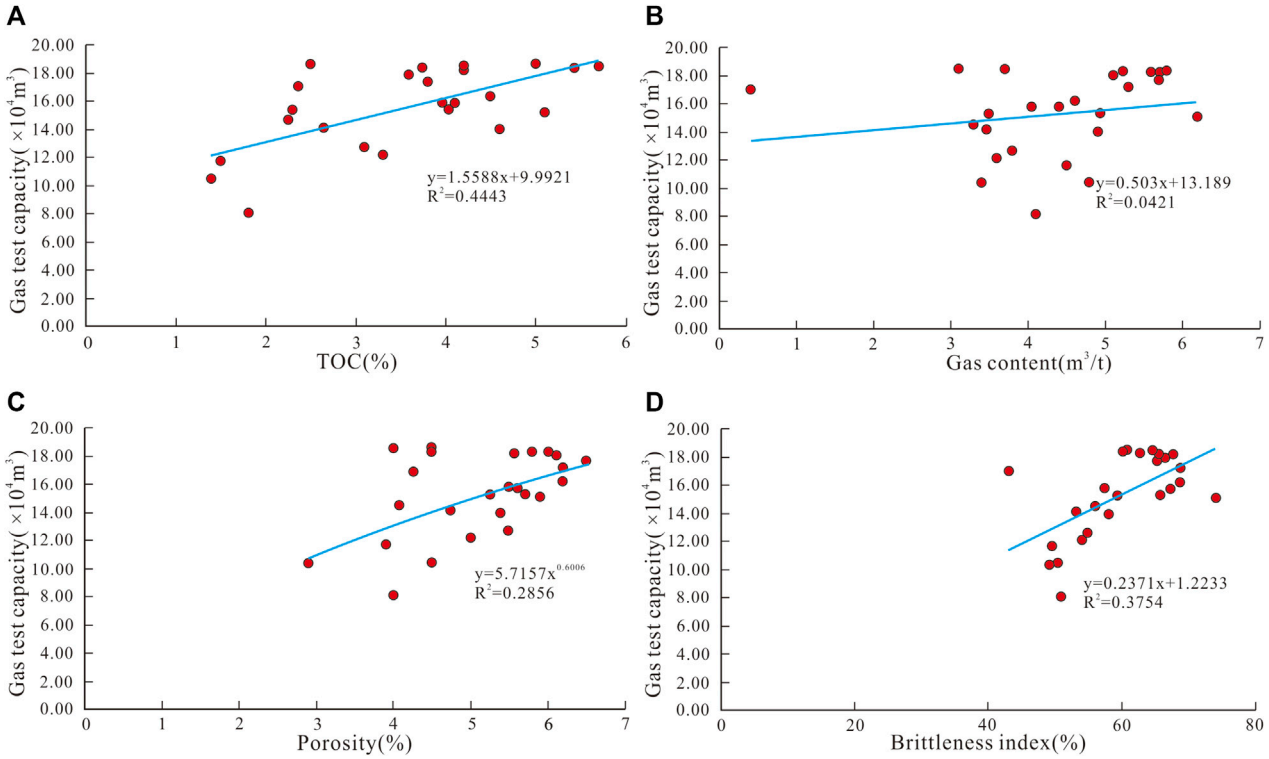

FIGURE 11 | Relationship between test production below 200,000 m^3 and reservoir physical properties in the study area.

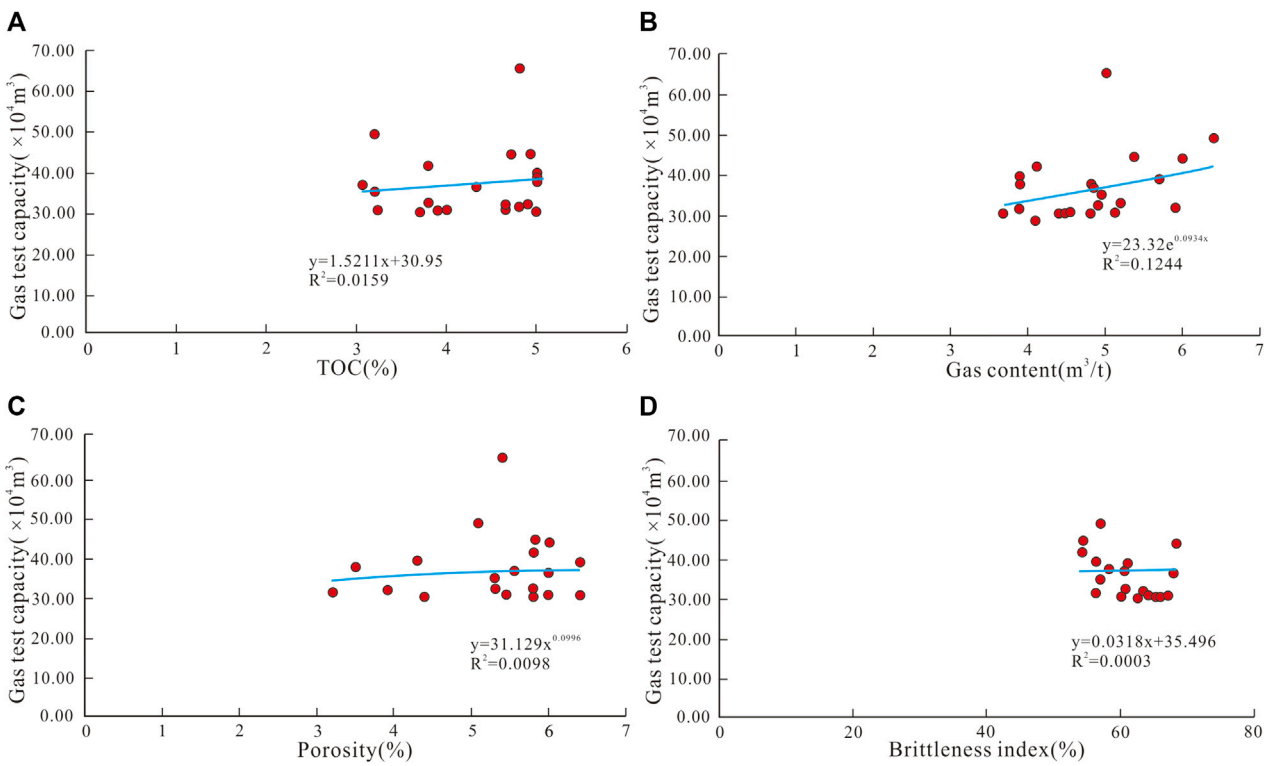

FIGURE 12 | Relationship between test production above 300,000 m^3 and reservoir physical properties in the study area.

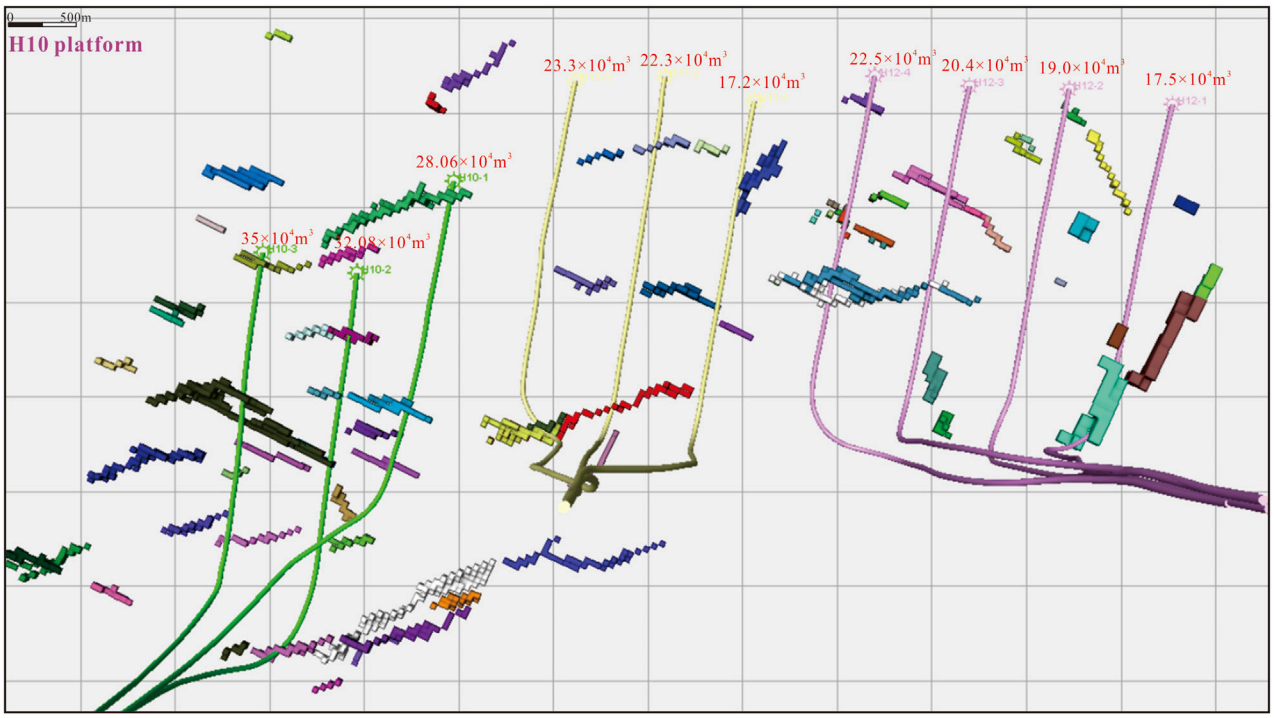

FIGURE 13 | Relationship between fracture development area and test productivity.

DISCUSSION

Controlling Factors of Deep Shale Gas Enrichment and Yield

Sedimentary Facies Are the Main Factor Controlling the Development of Shale Gas Reservoirs

1) An anoxic deep-water strongly reducing environment is a necessary condition for OM enrichment

The reducibility of sedimentary water strongly affects the preservation of OM, and an anoxic strong reduction environment is more conducive to the enrichment and preservation of OM (Loucks et al., 2009; Cheng et al., 2021). Trace element analysis showed that the U/Th ratio of the small layer 1 is > 1.25, making it a strongly reducing environment of residual hypoxia, an important and favorable feature for sweet-spot layers. The core analysis data show good positive

TABLE 3 | Comprehensive evaluation standard of selecting shale gas areas in the study area.

Evaluation parameter	Weight grade	Weight	Classification and evaluation criteria of shale gas reservoir logging		
			Class I	Class II	Class III
Total Gas Volume (m^3/t)	Level 1	0.3	>3	2–3	<2
TOC (%)	Level 2	0.3	>3	2–3	<2
Porosity (%)	Level 2	0.2	>5	3–5	<3
Brittleness Index (%)	Level 2	0.2	>55	35–55	<35

TABLE 4 | Classification standards of favorable areas in the study area.

Classification	Burial depth	The thickness of class I + II reservoirs	Reservoir evaluation index	Structural development
Class I	Below 4,000 m	>40 m	>1.4	The fault is undeveloped, and the structure is relatively simple
Class II	4000–4500 m	25–40 m	1.2–1.4	The fault is undeveloped, and the structure is relatively simple
Class III	4000–4500 m	<25 m	<1.2	Fault development

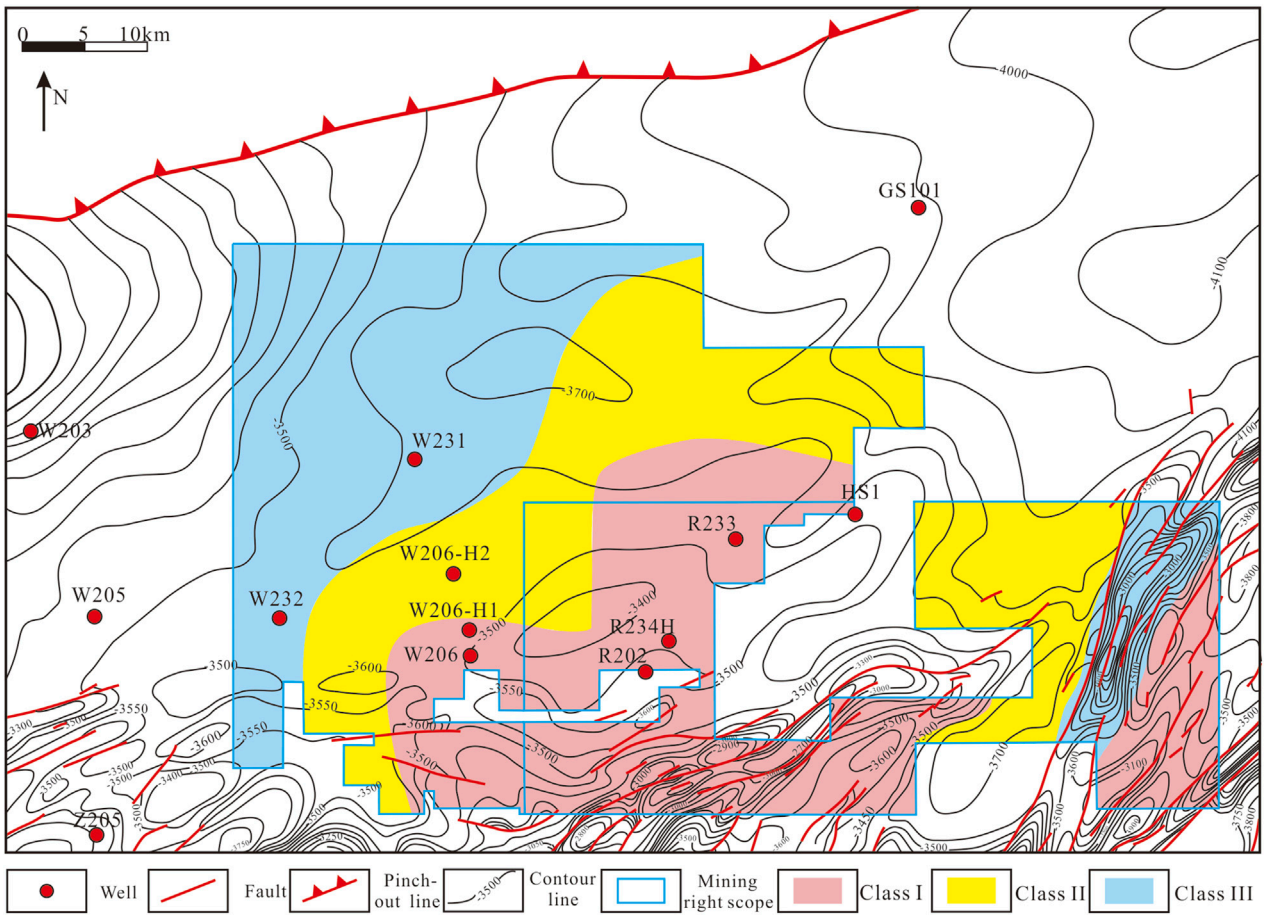

FIGURE 14 | Favorable target areas in the study area.

correlations between TOC and the V/Cr, U/Th, and Ni/Co values of trace elements, with corresponding coefficients of determination (R^2) of 0.4141, 0.4794, and 0.6418 (**Figure 8**). The higher the R^2, the more anoxic the sedimentary environment of the formation will be, and the more OM will be enriched.

2) The OM content and maturity are the key factors affecting the physical properties and gas-bearing of shale gas reservoirs

OM is the material source of shale gas. Thermal maturation makes OM generate many hydrocarbons after reaching the hydrocarbon generation threshold. After OM generates hydrocarbon, it begets high-pressure protective pores and forms organic pores in the process of hydrocarbon generation, which increases the rock's porosity. At the same time, the reduction in OM volume could produce ultrafine fractures, which is conducive to the preservation of shale gas. Many micropores and microfractures are generated in the process of hydrocarbon generation, and more free natural gas is stored in these spaces. The higher the TOC content, the larger the total volume of pores, and the larger the specific surface area available for adsorption of adsorbed gas. Thus, the total gas volume of the shale will grow. The core analysis and test data of 11 wells (including W203, W205, W206, and R233H) show that the TOC content has positive correlations with porosity, quartz, and gas content (**Figure 9**), which also confirms the positive role of OM in shale reservoir space and gas-bearing property.

3) Organic rich siliceous mud shelves and organic-rich mud shelves are the most favorable sedimentary microfacies for shale gas enrichment

The results of sedimentary microfacies analysis show that deep-water silty mud shelves, organic-rich silty mud shelves, organic-rich siliceous mud shelves, and organic-rich mud shelves in the outer shelf subfacies are the favorable microfacies for shale gas exploration and development. Among them, organic-rich siliceous mud shelves and organic-rich mud shelves are the most favorable microfacies owing to the following characteristics: high TOC content, with an average of 5%, giving them better hydrocarbon generation potential and more abundant shale gas resources; more developed pores, with an average porosity of 6%, providing enough reservoir space for shale gas enrichment; more developed shale interlayer foliation

fractures; medium-carbon and high-carbon siliceous shale facies with their high brittle mineral contents and low carbonate mineral contents (mostly less than 10%); a high biogenic silica content, greater than 45%, which is conducive to improving the hydrofracture effect of shale (**Table 2**).

Fracture Development Is the Key Factor for Achieving a High Yield of Shale Gas

Fractures are important reservoir spaces and migration channels of shale gas, playing an important role in the accumulation, preservation, exploration, and development of shale gas (Li et al., 2019c; Li et al., 2020; Li H. et al., 2021; Li 2021). Investigation of the Lower Paleozoic marine shale gas in the Sichuan Basin and its surrounding areas shows that marine shale has a good material foundation, and gas-bearing can almost be observed in each drilling. Still, the gas drilling results are very different. Therefore, the preservation conditions are key factors in determining whether shale gas can be enriched and produced. The shale gas area in North America is characterized by weak structural activity and developed horizontal fractures. Most of the shale gas is enriched in shale reservoirs uniformly (**Figure 10A**). Therefore, good single-well production can often be realized through fracturing and reconstruction of the reservoir. However, China's shale gas enrichment modes are mainly anticlinal and synclinal structural modes, and both are found in the study area (**Figures 10B,C**). Therefore, fully sealing the top and floor of the reservoir is very important for reservoir formation, and the fracture is the key to the sealing effect. If the fracture or fault is not developed at the high point of the syncline or anticline structure, the shale gas may not be lost, and the fracture could play a positive role in the accumulation of shale gas. The shale gas of the anticline structure is accumulated in the core of the anticline, while the syncline structure is concentrated in the syncline wings.

According to the correlation between the test product and the four property parameters of the reservoir in the study area, test production of less than 200,000 m^3 in a well positively correlates with the reservoir's physical properties. In contrast, the presence of a test production of more than 300,000 m^3 has a poor correlation with the reservoir's physical properties (**Figures 11**, **12**). Therefore, the development of fractures is often a direct manifestation of the poor correlation with reservoir physical properties. As the gas test production is related to geological and engineering factors, geological factors determine the shale gas enrichment, and engineering factors play an important role in improving the test production. Different fracturing and mining methods will lead to different test production in the same area. Therefore, the correlation coefficient (R^2) is small in **Figures 11**, **12**, proving that their correlation is weak. The phenomenon is normal. In addition, according to the seismic prediction results of the fracture development zone, most of the class I wells with a test production of more than 300,000 m^3 are located in areas with relatively well-developed fractures. The comparison between the test productivity data and the micro-seismic fracture monitoring data also shows that the test productivity of shale gas production wells in the fracture development area is generally larger than that in the area where fractures are not developed (**Figure 13**).

Selection of Favorable Target Areas

According to the evaluation indices for choosing shale gas areas in China and abroad, combined with the existing research results in Southern Sichuan and the actual situation of the study area, seven evaluation parameters, such as gas volume, pressure coefficient, porosity, brittle mineral content, high-quality shale thickness, burial depth, and TOC, were selected as the main evaluation indices for the selection of favorable areas. The evaluation standards for determining shale gas areas in the study area were formulated (**Table 3**). The combination of these with the location parameters, such as structure, preservation conditions, burial depth, and class I + II reservoir thickness, the classification standards of favorable areas in the study area was formulated (**Table 4**), and finally, the study area was divided into class I, II, and III favorable areas (**Figure 14**).

Class I favorable areas are a class I + II reservoirs with a thickness of more than 40 m, a reservoir index of more than 1.4, undeveloped faults, and a relatively simple structure. They lack surface nonworking areas, have a burial depth of less than 4,000 m, and are mainly distributed in the south of wells W206, W206H1, R234H, R233H, and some areas in the east of the study area.

Class II favorable areas are the areas with reservoir thickness greater than 25 m, reservoir index greater than 1.2, undeveloped faults, and a relatively simple structure. They lack nonworking ground areas, have a burial depth of less than 4,500 m, and are mainly distributed in the north of well W206H1 in the middle of the study area, a belt running through the north and south of the area where Well W206H2 is located, and the northeast of North Rongchang block.

The class III favorable areas are those with reservoir thickness less than 25 m, either with or without fracture development. They are located in the Xishan/Luoguanshan structural belt, lack ground nonworking areas, are buried within a small layer at 4,500 m, and are mainly distributed in the northwest of well W232 and well W231 in the study area.

CONCLUSION

Taking the Long 1_1 sub-member of the Wufeng Formation of the Upper Ordovician and the Longmaxi Formation of the Lower Silurian in the East Weiyuan–North Rongchang area as an example, this paper comprehensively studies the geological characteristics and controlling factors of the enrichment and high-yield of deep shale gas by XRD analysis, LECO TOC-S analysis, optical microscopy, and AIP-FESEM and identified the favorable target areas for shale gas development in the study area. The main findings and conclusions are as follows:

1) In the study area, the brittle minerals of the Long 1_1 sub-member of the Wufeng Formation–Longmaxi Formation are mainly quartz, feldspar, carbonate minerals, pyrite, and hematite. The OM is in the over mature stage, and the TOC content is high, primarily producing dry gas. Vertically, the maturity of brittle minerals and OM and TOC contents gradually increases from top to bottom, the small layer 1 having the most.

2) The reservoir space of the Long 1_1 sub-member of the Wufeng Formation–Longmaxi Formation in the study area mainly includes organic pores, inorganic pores, and fractures. The inorganic pores are mainly intercrystalline, intercrystalline dissolved pores, and intergranular pores. Organic pores and fractures are important seepage channels of shale gas, and microfractures can better connect inorganic and organic pores. According to the frequency distribution curve of pore radii, the pore structure can be divided into the unimodal type, bimodal type, monoclinic type I, and monoclinic type II. The unimodal type is the best, with small pores predominating, followed by mesopores and the developed organic pores. The unimodal type has high OM content, good sortability, and good connectivity.
3) Considering the redox environment, sedimentary facies, lithofacies, reservoir characteristics, and other factors, the sedimentary facies is the main thing controlling the development of shale gas reservoirs in the study area. The organic-rich siliceous mud shelf microfacies, organic-rich mud shelf facies, and high-carbon siliceous shale facies deposited in deep-water strongly reducing environments are the most favorable areas for developing shale gas reservoirs. Under favorable reservoir conditions, the development of fractures is the key factor in obtaining high shale gas yields.
4) Combining the reservoir evaluation index, burial depth, class I + II reservoir distribution, and structural development in the study area, we identified the favorable exploration target areas in the study area. In the class I areas, the reservoir thickness is greater than 40 m, the reservoir index is greater than 1.4, the fault is not developed, and the structure is relatively simple. The class I areas are mainly distributed in W206, W206H1, R234H, and R233H and areas to its south and some areas in the east of the study area.

DATA AVAILABILITY STATEMENT

The original contributions presented in the study are included in the article/supplementary material, further inquiries can be directed to the corresponding author.

AUTHOR CONTRIBUTIONS

YW contributed in writing, reviewing, and editing, data curation, writing-original draft preparation; JL, ZG, BY, CY and TT contributed in formal analysis, validation, and methodology, supervision, project administration; HT contributed to visualization and investigation.

REFERENCES

Cai, S. Y., Xiao, Q. L., Zhu, W. P., Wang, X. L., Yuan, H., Chen, J., et al. (2020). Characteristics and Controlling Factors of Nano Pores in Shale Reservoirs of Wufeng-Longmaxi Formations in Southern Sichuan Basin:insights from Shuanghe Outcrop in Changning Area. *Petrol. Geol. Exp.* 42 (6), 920–927. doi:10.11781/sysydz202006920

Chai, J., Ouyang, Y. B., and Zhang, D. D. (2020). Crackdetection Method in Similar Material Models Based on DIC. *J. Min. Strata Control. Eng.* 2 (2), 023015. doi:10.13532/j.jmsce.cn10-1638/td.2020.02.003

Chen, F., Zheng, Q., Ding, X., Lu, S., and Zhao, H. (2020b). Pore Size Distributions Contributed by OM, clay and Other Minerals in Over-mature marine Shale: A Case Study of the Longmaxi Shale from Southeast Chongqing, China. *Mar. Pet. Geology.* 122, 104679. doi:10.1016/j.marpetgeo.2020.104679

Chen, S., Han, Y., Fu, C., Zhang, H., Zhu, Y., and Zuo, Z. (2016). Micro and Nano-Size Pores of clay Minerals in Shale Reservoirs: Implication for the Accumulation of Shale Gas. *Sediment. Geology.* 342, 180–190. doi:10.1016/j.sedgeo.2016.06.022

Chen, S. L., Huang, B. X., Li, D., Zhao, X. L., Xu, J., and Wang, C. W. (2020a). Experiment Study on the Basic Law of High Pressure Abrasive Hydraulic Cutting for Coal-Rock Mass. *J. Min. Strata Control. Eng.* 2 (4), 047521. doi:10.13532/j.jmsce.cn10-1638/td.20200506.002

Chen, S., Liu, P., Tang, D., Tao, S., and Zhang, T. (2021a). Identification of Thin-Layer Coal Texture Using Geophysical Logging Data: Investigation by Wavelet Transform and Linear Discrimination Analysis. *Int. J. Coal Geology.* 239, 103727. doi:10.1016/j.coal.2021.103727

Chen, S., Tang, D., Tao, S., Liu, P., and Mathews, J. P. (2021b). Implications of the *In Situ* Stress Distribution for Coalbed Methane Zonation and Hydraulic Fracturing in Multiple Seams, Western Guizhou, China. *J Pet. Sci. Eng.* 204, 108755. doi:10.1016/j.petrol.2021.108755

Cheng, L., Guan, F. J., Liu, D. H., Yang, W. X., and Sun, J. (2021). Micropore Characteristics and Geological Significance of Shale Reservoirs: Case Study of Fuling Shale Gas in Sichuan Basin, China. *Geofluids*, 6636156. doi:10.1155/2021/6636156

Curtis, M. E., Cardott, B. J., Sondergeld, C. H., and Rai, C. S. (2012). Development of Organic Porosity in the Woodford Shale with Increasing thermal Maturity. *Int. J. Coal Geology.* 103, 26–31. doi:10.1016/j.coal.2012.08.004

Fan, C. H., He, S., Zhang, Y., Qin, Q. R., and Zhong, C. (2018). Development Phases and Mechanisms of Tectonic Fractures in the Longmaxi Formation Shale of the Dingshan Area in Southeast Sichuan Basin, China. *Acta Geol. Sin* 92 (6), 2351–2366. doi:10.1111/1755-6724.13732

Fan, C., Li, H., Qin, Q., He, S., and Zhong, C. (2020b). Geological Conditions and Exploration Potential of Shale Gas Reservoir in Wufeng and Longmaxi Formation of southeastern Sichuan Basin, China. *J Pet. Sci. Eng.* 191, 107138. doi:10.1016/j.petrol.2020.107138

Fan, C., Li, H., Zhao, S., Qin, Q., Fan, Y., Wu, J., et al. (2020a). Formation Stages and Evolution Patterns of Structural Fractures in Marine Shale: Case Study of the Lower Silurian Longmaxi Formation in the Changning Area of the Southern Sichuan Basin, China. *Energy Fuels* 34, 9524–9539. doi:10.1021/acs.energyfuels.0c01748

Guo, H., He, R., Jia, W., Peng, P. a., Lei, Y., Luo, X., et al. (2018). Pore Characteristics of Lacustrine Shale within the Oil Window in the Upper Triassic Yanchang Formation, southeastern Ordos Basin, China. *Mar. Pet. Geology.* 91, 279–296. doi:10.1016/j.marpetgeo.2018.01.013

Han, H., Pang, P., Li, Z.-l., Shi, P.-t., Guo, C., Liu, Y., et al. (2019). Controls of Organic and Inorganic Compositions on Pore Structure of Lacustrine Shales of Chang 7 Member from Triassic Yanchang Formation in the Ordos Basin, China. *Mar. Pet. Geology.* 100, 270–284. doi:10.1016/j.marpetgeo.2018.10.038

He, S., Li, H., Qin, Q. R., and Long, S. X. (2021b). Effects of Dissolved Organic Matter on Shale Pore Structure of Low-Mature Lacustrine Facies Organic-Rich Shale. *Energy Source A* 9. doi:10.1080/15567036.2021.1979694

He, S., Li, H., Qin, Q., and Long, S. (2021a). Influence of Mineral Compositions on Shale Pore Development of Longmaxi Formation in the Dingshan Area, Southeastern Sichuan Basin, China. *Energy Fuels* 35 (13), 10551–10561. doi:10.1021/acs.energyfuels.1c01026

He, S., Li, H., Qin, Q. R., and Long, S. X. (2021d). Influence of mineral Compositions on Shale Pore Development of Longmaxi Formation in the Dingshan Area, Southeastern Sichuan Basin, China. *Energy Fuel* 191, 107138. doi:10.1021/acs.energyfuels.1c01026

He, X., Li, W. G., Dang, L. R., Huang, S., Wang, X. D., Zhang, C. L., et al. (2021c). Key Technological Challenges and Research Directions of Deep Shale Gas

Development. *Nat. Gas Ind.* 41 (1), 118–124. doi:10.3787/j.issn.1000-0976.2021.01.010

Huang, F. R., Yan, S. X., Wang, X. L., Jiang, P. C., and Zhan, S. B. (2021). Study on Infrared Radiation Characteristics of Gneiss under Uniaxial Compression. *J. Min. Strata Control. Eng.* 3 (1), 013011. doi:10.13532/j.jmsce.cn10-1638/td.20200730.001

Jarvie, D. M., Hill, R. J., Ruble, T. E., and Pollastro, R. M. (2007). Unconventional Shale-Gas Systems: The Mississippian Barnett Shale of north-central Texas as One Model for Thermogenic Shale-Gas Assessment. *Bulletin* 91 (4), 475–499. doi:10.1306/12190606068

Ko, L. T., Loucks, R. G., and Milliken, K. L. (2017). Controls on Pore Types and Pore-Size Distribution in the Upper Triassic Yanchang Formation, Ordos Basin, China: Implications for Pore-Evolution Models of Lacustrine Mudrocks. *Interpretation* 5, SF127–SF147. doi:10.1190/int-2016-0115.1

Li, H., Qin, Q., Zhang, B., Ge, X., Hu, X., Fan, C., et al. (2020). Tectonic Fracture Formation and Distribution in Ultradeep Marine Carbonate Gas Reservoirs: A Case Study of the Maokou Formation in the Jiulongshan Gas Field, Sichuan Basin, Southwest China. *Energy Fuels* 34, 14132–14146. doi:10.1021/acs.energyfuels.0c03327

Li, H. (2021). Quantitative Prediction of Complex Tectonic Fractures in the Tight sandstone Reservoirs: a Fractal Method. *Arab. J. Geosci.* 14 (19), 1986. doi:10.1007/s12517-021-08344-0

Li, H., Tang, H. M., and Zheng, M. J. (2019). Micropore Structural Heterogeneity of Siliceous Shale Reservoir of the Longmaxi Formation in the Southern Sichuan Basin, China. *Minerals* 9, 548. doi:10.3390/min9090548

Li, H., Tang, H., Qin, Q., Zhou, J., Qin, Z., Fan, C., et al. (2019c). Characteristics, Formation Periods and Genetic Mechanisms of Tectonic Fractures in the Tight Gas Sandstones Reservoir: A Case Study of Xujiahe Formation in YB Area, Sichuan Basin, China. *J Pet. Sci. Eng.* 178, 723–735. doi:10.1016/j.petrol.2019.04.007

Li, H., Wang, Q., Qin, Q., and Ge, X. (2021c). Characteristics of Natural Fractures in an Ultradeep Marine Carbonate Gas Reservoir and Their Impact on the Reservoir: A Case Study of the Maokou Formation of the JLS Structure in the Sichuan Basin, China. *Energy Fuels* 35 (16), 13098–13108. doi:10.1021/acs.energyfuels.1c01581

Li, W. G., Yue, H., Sun, Y. P., Guo, Y., Wu, T. P., Zhang, N. Q., et al. (2021b). Development Evaluation and Optimization of Deep Shale Gas Reservoir with Horizontal Wells Based on Production Data. *Geofluids*, 4815559. doi:10.1155/2021/4815559

Liu, J. S., Yang, H. M., Wu, X. F., and Liu, Y. (2020). The *In Situ* Stress Field and Microscale Controlling Factors in the Ordos Basin, central China. *Int. J. Rock Mech. Min* 135, 104488. doi:10.1016/j.ijrmms.2020.104482

Liu, J., Yang, H., Bai, J., Wu, K., Zhang, G., Liu, Y., et al. (2021c). Numerical Simulation to Determine the Fracture Aperture in a Typical basin of China. *Fuel* 283, 118952. doi:10.1016/j.fuel.2020.118952

Liu, Q. Y., Zhu, H. Y., and Chen, P. J. (2021e). Research Progress and Direction of Geology-Engineering Integrated Drilling Technology: A Case Study on the Deep Shale Gas Reservoirs in the Sichuan Basin. *Nat. Gas Ind.* 41 (1), 178–188. doi:10.3787/j.issn.1000-0976.2021.01.016

Liu, S. G., Jiao, K., Zhang, J. C., Ye, Y. H., Xie, G. L., Deng, B., et al. (2021d). Research Progress on the Pore Characteristics of Deep Shale Gas Reservoirs: An Example from the Lower Paleozoic marine Shale in the Sichuan Basin. *Nat. Gas Ind.* 41 (1), 29–41. doi:10.3787/j.issn.1000-0976.2021.01.003

Liu, Y. J., Lai, F. Q., Zhang, H. J., Tan, Z. J., Wang, Y. F., and Tan, X. F. (2021a). A Novel mineral Composition Inversion Method of Deep Shale Gas Reservoir in Western Chongqing. *J. Petrol. Sci. Eng.* 202, 108528. doi:10.1016/j.petrol.2021.108528

Liu, Y. Y., Ma, X. H., Zhang, X. W., Wei, G., Kang, L. X., Yu, R. Z., et al. (2021b). Shale Gas Well Flowback Rate Prediction for Weiyuan Field Based on a Deep Learning Algorithm. *J. Petrol. Sci. Eng.* 203, 108637. doi:10.1016/j.petrol.2021.108637

Loucks, R. G., Reed, R. M., Ruppel, S. C., and Jarvie, D. M. (2009). Morphology, Genesis, and Distribution of Nanometer-Scale Pores in Siliceous Mudstones of the Mississippian Barnett Shale. *J. Sediment. Res.* 79 (12), 848–861. doi:10.2110/jsr.2009.092

Lyu, P. F., Ma, F., and Bao, X. Y. (2021). Experimental Study on Pore Microstructure and Methane Occurrence Characteristics of Shale of marine-continent Transition Phase. *Fresen. Environ. Bull.* 30 (1), 330–337.

Ma, X., Wang, H., Zhou, S., Shi, Z., and Zhang, L. (2021). Deep Shale Gas in China: Geological Characteristics and Development Strategies. *Energ. Rep.* 7, 1903–1914. doi:10.1016/j.egyr.2021.03.043

Nie, H. K., and Jin, Z. J. (2016). Source Rock and Cap Rock Controls on the Upper Ordovician Wufeng Formation-Lower Silurian Longmaxi Formation Shale Gas Accumulation in the Sichuan Basin and its Peripheral Areas. *Acta Geol. Sin* 90, 1059–1060. doi:10.1111/1755-6724.12752

Nie, H. K., Sun, C. X., Liu, G. X., Du, W., and He, Z. L. (2018). Dissolution Pore Types of the Wufeng Formation and the Longmaxi Formation in the Sichuan Basin, South China: Implications for Shale Gas Enrichment. *Mar. Petrol. Geol.* 101, 243–251. doi:10.1016/j.marpetgeo.2018.11.042

Rashid, F., Hussein, D., Hussein, D., Lawrence, J. A., and Khanaqa, P. (2020). Characterization and Impact on Reservoir Quality of Fractures in the Cretaceous Qamchuqa Formation, Zagros Folded belt. *Mar. Pet. Geology.* 113, 104117. doi:10.1016/j.marpetgeo.2019.104117

Rui, J., Zhang, H., Zhang, D., Han, F., and Guo, Q. (2019). Total Organic Carbon Content Prediction Based on Support-Vector-Regression Machine with Particle Swarm Optimization. *J Pet. Sci. Eng.* 180, 699–706. doi:10.1016/j.petrol.2019.06.014

Sakhaee-Pour, A., and Bryant, S. L. (2015). Pore Structure of Shale. *Fuel* 143, 467–475. doi:10.1016/j.fuel.2014.11.053

Shi, X., Wang, J., Liu, G., Yang, L., Ge, X., and Jiang, S. (2016). Application of Extreme Learning Machine and Neural Networks in Total Organic Carbon Content Prediction in Organic Shale with Wire Line Logs. *J. Nat. Gas Sci. Eng.* 33, 687–702. doi:10.1016/j.jngse.2016.05.060

Song, L., Bhattacharya, S., Webb, Z., Fowler, A., and Lee, V. (2021). Preservation of organic carbon in the Cretaceous Hue Shale on the North Slope of Alaska: Insights from pyrite morphology. *International Journal of Coal Geology* 235, 103678. doi:10.1016/j.coal.2021.103678

Sun, S.Y (2021). Study on the characteristics of continental shale reservoir and the calculation of relative permeability curve. *Fresen. Environ. Bull.* 30 (4A), 4620–4627.

Tabatabaei, H (2021). Analysis of fracture density and their effect on mud loss in Asmari reservoir via FMI/FMS log, Rag-e-Safid oil field, SW of Iran. *Himal. Geol.* 42 (1), 205–210.

Wang, C., Shi, W.Z., Zhang, X.M., Xu, Z, Yuan, Q, and Xiao, D (2017). Comprehensive evaluation of fracture system in shale reservoir and its influence on shale gas seepage and accumulation. *Petrol. Geol. Rec. Effic* 24 (1), 50–56. doi:10.13673/j.cnki.cn37-1359/te.2017.01.007

Wang, H.B., Zhou, T., and Huang, X (2021). Pore evolution and fractal dimension characteristics of shale with different maturity. *Fresen. Environ. Bull.* 30 (6B), 7596–7603.

Wang, H., Wu, W., Chen, T., Dong, X., and Wang, G. (2019). An Improved Neural Network for TOC, S1 and S2 Estimation Based on Conventional Well Logs. *J. Pet. Sci. Eng.* 176, 664–678. doi:10.1016/j.petrol.2019.01.096

Wang, P., Chen, Z., Pang, X., Hu, K., Sun, M., and Chen, X. (2016). Revised Models for Determining TOC in Shale Play: Example from Devonian Duvernay Shale, Western Canada Sedimentary basin. *Mar. Pet. Geology.* 70, 304–319. doi:10.1016/j.marpetgeo.2015.11.023

Wu, Y. J., Tang, H. M., Wang, Y., Li, J., Zeng, Y. X., Jiang, S. L., et al. (2021). Sedimentary Facies of the Longmaxi Formation Shale Gas Reservoir in the Weiyuan Area Based on Elemental Characteristics. *Geofluids*, 5021298. doi:10.1155/2021/5021298

Xi, Y., Jiang, J., Li, J., Li, H., and Gao, D. (2021b). Research on the Influence of Strike-Slip Fault Slippage on Production Casing and Control Methods and Engineering Application during Multistage Fracturing in Deep Shale Gas wells. *Energ. Rep.* 7, 2989–2998. doi:10.1016/j.egyr.2021.05.039

Xi, Y., Lian, W., Fan, L., Tao, Q., and Guo, X. (2021a). Research and Engineering Application of Pre-stressed Cementing Technology for Preventing Micro-annulus Caused by Cyclic Loading-Unloading in Deep Shale Gas Horizontal wells. *J. Pet. Sci. Eng.* 200, 108359. doi:10.1016/j.petrol.2021.108359

Xiao, D., Cao, J., Luo, B., Zhang, Y., Xie, C., Chen, S., et al. (2020). Mechanism of Ultra-deep Gas Accumulation at Thrust Fronts in the Longmenshan Mountains, Lower Permian Sichuan Basin, China. *J. Nat. Gas Sci. Eng.* 83, 103533. doi:10.1016/j.jngse.2020.103533

Xiong, L., Pang, H. Q., Zhao, Y., Wei, L. M., Zhou, H., and Cao, Q. (2021). Micro Pore Structure Characterization and Classification Evaluation of Reservoirs in Weirong Deep Shale Gas Field. *Reserv. Eval. Dev.* 11 (2), 20–29. doi:10.13809/j.cnki.cn32-1825/te.2021.02.003

Xu, F. S., Wang, F. P., Zhang, J. T., Fu, B., Zhang, Y., Yang, P. C., et al. (2021a). Strategies for Scale Benefit Development of Deep Shale Gas in China. *Nat. Gas Ind.* 41 (1), 205–213. doi:10.3787/j.issn.1000-0976.2021.01.019

Xu, N. Z., and Gao, C. (2020). Study on the Special Rules of Surface Subsidence Affected by normal Faults. *J. Min Strata Control. Eng.* 2 (1), 011007. doi:10.13532/j.jmsce.cn10-1638/td.2020.01.011

Xu, Z., Pengn, N. J., Shi, W. Z., and Shu, Z. G. (2021b). Reservoir Fracture Characteristics and Controlling Factors of Shale Gas of Wufeng-Longmaxi Formation in Fuling Area. *J. East. China Univ. Tech.* 44 (3), 267–279. doi:10.3969/j.issn.1674-3504.2021.03.008

Yin, S., Han, C., Wu, Z., and Li, Q. (2019). Developmental Characteristics, Influencing Factors and Prediction of Fractures for a Tight Gas sandstone in a Gentle Structural Area of the Ordos Basin, China. *J. Nat. Gas Sci. Eng.* 72, 103032. doi:10.1016/j.jngse.2019.103032

Yin, S., and Wu, Z. (2020). Geomechanical Simulation of Low-Order Fracture of Tight sandstone. *Mar. Pet. Geology.* 117, 104359. doi:10.1016/j.marpetgeo.2020.104359

Yu, H., Rezaee, R., Wang, Z., Han, T., Zhang, Y., Arif, M., et al. (2017a). A New Method for TOC Estimation in Tight Shale Gas Reservoirs. *Int. J. Coal Geology.* 179, 269–277. doi:10.1016/j.coal.2017.06.011

Yu, Y., Luo, X., Lei, Y., Wang, X. Z., Wang, X., Zhang, L., et al. (2016). Characterization of Lacustrine Shale Pore Structure: The Upper-Triassic Yanchang Formation, Ordos Basin, China. *J. Nat. Gas Geosci.* 1, 299–308. doi:10.1016/j.jnggs.2016.10.001

Yu, Y. X., Luo, X. R., and Cheng, M. (2017b). Study on the Distribution of Extractable Organic Matter in Pores of Lacustrine Shale: An Example of Zhangjiatan Shale from the Upper Triassic Yanchang Formation. *Ordos Basin, China. Interpretation* 5, SF109–SF126. doi:10.1190/INT-2016-0124.1

Yuan, Y. Y., Li, H., Wang, Q., and Zhong, M. Y. (2021). Influence of Different thermal Evolution Stages on Shale Pore Development. *Energy Source Part A*. doi:10.1080/15567036.2021.1942333

Zhang, B. L., Shen, B. T., Zhang, J. H., and Zhang, X. G. (2020a). Experimental Study of Edge-Opened Cracks Propagation in Rocklike Materials. *J. Min. Strata Control. Eng.* 2 (3), 033035. doi:10.13532/j.jmsce.cn10-1638/td.20200313.001

Zhang, D. D., Li, S. J., Zhang, X., Yang, Y. Y., and Chai, J. (2020b). Experimental Study on Mining Fault Activation Characteristics by a Distributed Optical Fiber System. *J. Min. Strata Control. Eng.* 2 (1), 013018. doi:10.13532/j.jmsce.cn10-1638/td.2020.01.010

Zhang, F., Jiang, Z., Sun, W., Zhang, X., Zhu, L., Li, X., et al. (2020c). Effect of Microscopic Pore-Throat Heterogeneity on Gas-phase Percolation Capacity of Tight sandstone Reservoirs. *Energy Fuels* 34 (10), 12399–12416. doi:10.1021/acs.energyfuels.0c02393

Zhang, K., Jia, C., Song, Y., Jiang, S., Jiang, Z., Wen, M., et al. (2020d). Analysis of Lower Cambrian Shale Gas Composition, Source and Accumulation Pattern in Different Tectonic Backgrounds: A Case Study of Weiyuan Block in the Upper Yangtze Region and Xiuwu Basin in the Lower Yangtze Region. *Fuel* 263, 115978. doi:10.1016/j.fuel.2019.115978

Zhang, N., Han, C., and Xie, Z. (2019). Theory of Continuous Beam Control and High Efficiency Supporting Technology in Coal Roadway. *J. Min Strat Control. Eng.* 1 (1), 013005. doi:10.13532/j.jmsce.cn10-1638/td.2019.02.004

Zhang, X. F., Qu, X. C., and Wei, Q. D. (2021). Development and Application of Multi-Dimension Multi-Parameter Monitoring and Early Warning Platform of Coal Bursts. *J. Min Strata Control. Eng.* 3 (1), 013013. doi:10.13532/j.jmsce.cn10-1638/td.20200922.002

Zhao, K. K., Jiang, P. F., Feng, Y. J., Sun, X. D., Cheng, L. X., and Zheng, J. W. (2020). Investigation of the Characteristics of Hydraulic Fracture Initiation by Using Maximum Tangential Stress Criterion. *J. Min Strata Control. Eng.* 3 (2), 023520. doi:10.13532/j.jmsce.cn10-1638/td.20201217.001

Zhao, P., Ma, H., Rasouli, V., Liu, W., Cai, J., and Huang, Z. (2017). An Improved Model for Estimating the TOC in Shale Formations. *Mar. Pet. Geology.* 83, 174–183. doi:10.1016/j.marpetgeo.2017.03.018

Zhao, Y., Li, N. Y., Yang, J., and Cheng, S. S. (2021). Optimization of Deep Shale Gas Well Spacing Based on Geology-Engineering Integration: A Case Study of Weirong Shale Gas Field. *Reserv. Eval. Dev.* 11 (3), 340–347. doi:10.13809/j.cnki.cn32-1825/te.2021.03.008

Zhou, D., Zheng, P., He, P., and Peng, J. (2016). Hydraulic Fracture Propagation Direction during Volume Fracturing in Unconventional Reservoirs. *J. Pet. Sci. Eng.* 141, 82–89. doi:10.1016/j.petrol.2016.01.028

Zhou, G., Gu, Z., Hu, Z., Chang, J., Duan, X., Liu, X., et al. (2020). Characterization and Interpretation of Organic Matter, clay Minerals, and Gas Shale Rocks with Low-Field NMR. *J. Pet. Sci. Eng.* 195, 107926. doi:10.1016/j.petrol.2020.107926

Zhou, H., Wei, L. M., Wang, T., Wang, Y., Pang, H. Q., and Zhang, T. C. (2021). Evaluation Method of Weirong Deep Shale Gas Reservoir and its Application. *Reserv. Eval. Dev.* 11 (2), 42–49. doi:10.13809/j.cnki.cn32-1825/te.2021.02.005

Zhu, W. C., Niu, L. L., Li, S. H., and Li, S. (2019). Creep-impact Test of Rock: Status-Of-The-Art and prospect. *J. Min. Strata Control. Eng.* 1 (1), 013003. doi:10.13532/j.jmsce.cn10-1638/td.2019.02.007

Zou, C., Zhang, X., Luo, P., Wang, L., Luo, Z., and Liu, L. (2010). Shallow-lacustrine Sand-Rich Deltaic Depositional Cycles and Sequence Stratigraphy of the Upper Triassic Yanchang Formation, Ordos Basin, China. *Basin Res.* 22, 108–125. doi:10.1111/j.1365-2117.2009.00450.x

Conflict of Interest: The authors declare that the research was conducted in the absence of any commercial or financial relationships that could be construed as a potential conflict of interest.

Publisher's Note: All claims expressed in this article are solely those of the authors and do not necessarily represent those of their affiliated organizations, or those of the publisher, the editors and the reviewers. Any product that may be evaluated in this article, or claim that may be made by its manufacturer, is not guaranteed or endorsed by the publisher.